JOURNAL OF SOLID STATE CHEMISTRY 135, 59–69 (1998)
ARTICLE NO. SC977590

Formation of Nickel, Cobalt, Copper, and Iron Aluminates from α- and γ-Alumina-Supported Oxides: A Comparative Study

P. H. Bolt,*,† F. H. P. M. Habraken,*,[1] and J. W. Geus†

*Debye Institute, Department of Atomic and Interface Physics, Utrecht University, P.O. Box 80000, 3508 TA Utrecht, The Netherlands; and
†Debye Institute, Department of Inorganic Chemistry, Utrecht University, P.O. Box 80083, 3508 TB Utrecht, The Netherlands

Received December 30, 1996; in revised form August 6, 1997; accepted August 12, 1997

The rates of metal aluminate formation in MeO_x/Al_2O_3 systems (Me = Ni, Co, Cu, Fe) at 500–1000°C in O_2 or N_2 atmospheres were compared, using both α-Al_2O_3 and γ-Al_2O_3 substrates. Interfacial reaction to $MeAl_2O_4$ was assessed using Rutherford backscattering spectrometry and X-ray diffraction. The lateral homogeneity of the samples was investigated using scanning electron microscopy. The spinel formation rate follows the sequence $FeAl_2O_4 < NiAl_2O_4 < CoAl_2O_4 < CuAl_2O_4$. This is explained in terms of thermodynamic limitations ($FeAl_2O_4$) and site-preference energies ($CoAl_2O_4$, $NiAl_2O_4$). The fast reaction to copper aluminate was accompanied by a severe rupture of the top layer (~1 μm) of the substrate. Penetration of transition metal ions into γ-Al_2O_3 substrates is notable at considerably lower temperatures than with α-Al_2O_3 substrates, mainly due to grain boundary diffusion. Annealing conditions that favor the formation of transition metal cations of a low valency (Co^{2+}, Cu^{+}) are beneficial for reactions to aluminates.

INTRODUCTION

The formation of aluminum spinel compounds at high temperatures (1200°C and above) from the parent oxides was extensively studied in the sixties and seventies (1–5). Experiments with MeO/Al_2O_3 diffusion couples (mainly MgO and NiO) indicated that $MeAl_2O_4$ formation obeyed the parabolic growth rate law and proceeded by counter-diffusion of Me^{2+} and Al^{3+} ions if vapor phase transport of MeO was excluded. Because of the limited spatial resolution of the analysis techniques applied in these investigations (mainly electron probe microanalysis), high temperatures had to be applied to achieve relatively large diffusion distances and thus to grow rather thick spinel layers (micron scale).

In previous studies in our laboratories (6–9), we were able to extend the temperature range downward to about 1000°C for the NiO/Al_2O_3 system using Rutherford backscattering spectrometry. However, much less is known about the phenomena occurring at the MeO–Al_2O_3 interface at moderate temperatures (500–1000°C). Under such conditions, the interactions are limited to nanometer scales, but nevertheless they are very important in several fields of technology, e.g., heterogeneous catalysis, microelectronics, and advanced composites.

We therefore investigated the interaction of oxidized nickel, cobalt, copper, and iron layers with polycrystalline α- and γ-Al_2O_3 substrates at temperatures up to 1000°C using Rutherford backscattering spectrometry (RBS), X-ray diffraction (XRD), scanning electron microscopy (SEM), and UV–vis diffuse reflectance spectroscopy (DRS).

EXPERIMENTAL

Sample Preparation

Polycrystalline α-Al_2O_3 substrates (obtained from Gimex, Geldermalsen, The Netherlands) were cut into pieces of 7 × 12 mm, and cleaned from adhering organic impurities by rinsing with acetone and subsequent annealing in ambient air at 1200°C. Slices of γ-Al_2O_3 (13 mm diameter) were produced by pressing γ-Al_2O_3 powder (Al 4172, Engelhard, De Meern, The Netherlands) for 3 min at 590 MPa. These slices were calcined at 500°C in flowing 80% N_2/20%O_2 (3 h) prior to vapor deposition of the metal overlayers.

Nickel, cobalt, copper, and iron films (35–100 nm) were vacuum vapor-deposited onto these substrates from an α-Al_2O_3 crucible. The metal films were oxidized to metal oxides (usually at 700°C) in 80% N_2/20% O_2. Oxidation of a 100-nm Ni film results in a 170-nm-thick NiO film. For the other metal oxides, the corresponding layer thicknesses are (starting from a 100-nm metal layer) as follows: CoO, 175 nm; Co_3O_4, 200 nm; Cu_2O, 167 nm; CuO, 174 nm; Fe_3O_4, 210 nm; Fe_2O_3, 214 nm.

To study the reaction of the oxides with the Al_2O_3 substrates, the samples were kept at temperatures ranging from

[1] To whom correspondence should be addressed.

0022-4596/98 $25.00

800 to 1000°C in a gas flow of 100% O_2, 100% N_2, or 80% N_2/20% O_2 for various periods of time.

Analysis

RBs analysis was performed with $^4He^+$ ions. The primary energy was 2.87 MeV or 2.01 MeV. The incident beam was parallel to the surface normal, and the scattering angle was 170°.

X-ray diffractograms were recorded on a Philips PW 1050 diffractometer equipped with an Fe-Kα source ($\lambda = 1.93735$Å).

The lateral distribution of the transition metal atoms over the substrate was assessed with Cambridge Stereoscan 150S and CamScan 2 scanning electron microscopes. Both microscopes were equipped with detectors for secondary and backscattered electrons and with a Link AN 10000 X-ray analysis system with an energy-dispersive detector. The acceleration voltage was 20 kV. The samples were mounted on an aluminum stub with carbon glue. A carbon layer was vacuum vapor-deposited onto the samples to provide a conducting surface.

UV–vis DRS spectra were collected on a Perkin-Elmer lambda 7 spectrometer. The spectra were recorded against a $CaSO_4$ reference sample, with a scan speed of 4 nm/s and a 2-nm slit.

RESULTS

Cobalt Oxides on Alumina

Cobalt oxides on α-alumina. SEM images of the Co_3O_4/α-Al_2O_3 samples (not shown) revealed that the thin cobalt oxide overlayer was homogeneously distributed over the alumina grains. After annealing at 1000°C for 70 h, similar images were obtained, but the surface was slightly rougher.

Figure 1 shows (parts of) the RBS spectra of Co_3O_4/α-Al_2O_3 samples after calcination and after subsequent heat treatment at 1000°C in 80% N_2/20% O_2. The thickness of the deposited cobalt layers was 95 (Fig. 1a) and 48nm (Fig. 1b). Upon heat treatment of the samples at 1000°C, a shoulder at the low-energy side of the cobalt peak developed. At the same time, the high-energy side of the aluminum edge moved to higher energies. These two observations indicate the penetration of cobalt ions into the alumina substrate and/or aluminum ions into the cobalt oxide overlayer (7, 8).

XRD showed that annealing at 1000°C of the Co_3O_4/α-Al_2O_3 samples led to the appearance of $CoAl_2O_4$ diffraction peaks, at the cost of Co_3O_4. The sample that was kept at 1000°C for 20 h (Fig. 1a, dashed curve) mainly contained $CoAl_2O_4$ and only a small amount of Co_3O_4. Apparently, the solid-state reaction between cobalt oxide and alumina was almost completed after 20 h.

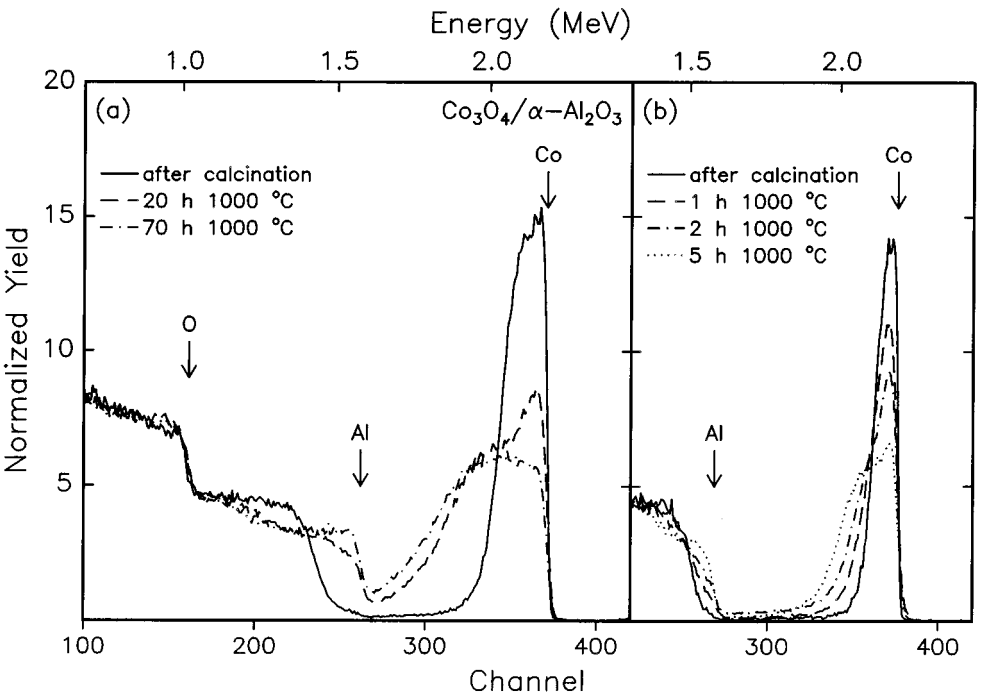

FIG. 1. Parts of the RBS spectra of Co_3O_4/α-Al_2O_3 samples recorded after annealing at 1000°C in N_2/20% O_2 for 0 –70 h. The arrows indicate the energy positions of surface scattering from the elements. The thickness of the deposited Co layer amounted to (a) 95 nm (190-nm Co_3O_4) and (b) 48 nm (96-nm Co_3O_4).

These findings are supported by DRS. Upon annealing at 1000°C, the characteristic absorption triplet at 545, 575, and 630 nm (10, 11) was found. Completely reacted samples had the characteristic bright blue color of $CoAl_2O_4$.

We thus conclude that the counterdiffusion of Co^{2+} and Al^{3+} ions, which was revealed by RBS (Fig. 1), led to the formation of $CoAl_2O_4$. After 1 h of annealing at 1000°C, this process has just started (Fig. 1b), but a small amount of aluminum was already present at the surface, as is evidenced by the small RBS yield at the Al surface energy position. Apparently, Al^{3+} ions rapidly diffuse toward the surface in the initial stage of the reaction, presumably along the boundaries of the cobalt oxide grains. After a long annealing period (70 h in Fig. 1a), the cobalt peak has substantially decreased and broadened; the shoulder has developed into a plateau. Further annealing had no measurable effect. Both XRD and RBS thus show that the reaction to cobalt aluminate has been completed in this sample. At the surface of the specimen, the Co/Al atomic ratio calculated from the RBS spectrum was 1/2.39. The deviation of this ratio from 1/2 (in $CoAl_2O_4$) is attributed to dilution of the $CoAl_2O_4$ with Al_2O_3 ($CoAl_2O_4 \cdot 0.20Al_2O_3$). Indeed, it has been reported that $CoAl_2O_4$ can accommodate up to 22 mol% Al_2O_3 in its lattice (12). The reaction to $CoAl_2O_4$ had almost completed after 20 h of annealing at 1000°C in the case of a 190-nm cobalt oxide overlayer (Fig. 1a). When the overlayer had half this thickness (Fig. 1b), the completion of the reaction was almost reached after only 5 h of annealing. This is in agreement with the power rate law. According to this law, the thickness of the reaction product layer is proportional to the square root of the annealing period (2).

Cobalt oxides on γ-alumina. In Fig. 2 the RBS spectra of a Co_3O_4/α-Al_2O_3 sample and a Co_3O_4/γ-Al_2O_3 sample after thermal treatment at 900°C in 80% N_2/20% O_2 are compared. It appears that the γ-Al_2O_3 substrate reacts (at 900°C) with cobalt oxide at a much higher rate than α-Al_2O_3: in 5 h most of the cobalt oxide on γ-Al_2O_3 has reacted to cobalt aluminate, whereas very little reaction took place in 20 h with the Co_3O_4/α-Al_2O_3 sample. SEM images of Co_3O_4/γ-Al_2O_3 samples kept at temperatures up to 900°C were similar to that of the bare substrate.

The presence of $CoAl_2O_4$ in the annealed Co_3O_4/γ-Al_2O_3 samples could not be established unequivocally by means of XRD. This is due to the fact that the $CoAl_2O_4$ diffraction peaks have almost the same positions as the rather broad γ-Al_2O_3 peaks. However, the enhancement of the relative intensities of the diffraction peaks at $d = 2.84$ and 2.43 Å and the appearance of the characteristic cobalt-blue color after sufficiently long annealing periods are strong indications for the formation of cobalt aluminate. Formation of α-Al_2O_3 was not observed after annealing at temperatures up to 900°C, but XRD demonstrated the presence of some θ-Al_2O_3 in the sample kept at 900°C for 5 h. Apparently, the transformation of γ-Al_2O_3 to θ-Al_2O_3 is accelerated by the presence of cobalt ions, since no signs of θ-Al_2O_3 were detected in the X-ray diffractograms of bare γ-Al_2O_3 slices kept at 900°C.

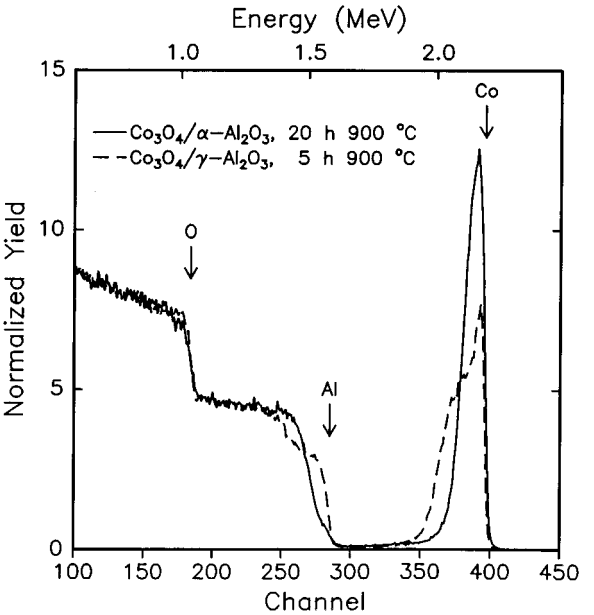

FIG. 2. RBS spectra of Co_3O_4/α-Al_2O_3 annealed at 900°C in N_2/20% O_2 for 20 h and Co_3O_4/γ-Al_2O_3 kept at 900°C for 5 h. The thickness of the deposited Co films amounted to about 40 nm.

Even at 800°C the penetration of cobalt atoms into the γ-Al_2O_3 substrate was notable. The RBS spectra (not shown) revealed a considerable change of the cobalt peak shape after 20 h of annealing. However, a second thermal treatment during an additional period of 20 h had hardly any effect. Apparently, the Co_3O_4/γ-Al_2O_3 system does not obey the parabolic growth rate law in the considered temperature range and annealing periods.

An α-Al_2O_3-supported 80-nm-thick Co_3O_4 layer (deposited Co layer: 40 nm) reacted completely to $CoAl_2O_4$ during annealing at 1000°C for 12 h (Fig. 3). A slight excess of Al_2O_3 was dissolved into the spinel phase (Co/Al = 1/2.06 in the near-surface region). The RBS spectrum of a similarly treated Co_3O_4/γ-Al_2O_3 sample (which had the same bright cobalt-blue color as the annealed Co_3O_4/α-Al_2O_3 sample) shows that the cobalt atoms penetrated much deeper into the γ-Al_2O_3 substrate than into the α-Al_2O_3. The Co/Al ratio at the surface is much lower (1/4.1), which is substantially below the composition that corresponds to the solubility limit of Al_2O_3 in $CoAl_2O_4$ at 1000°C (1/2.44). The cobalt concentration decreases slowly with increasing depth. Obviously, the processes that occur in the Co_3O_4/γ-Al_2O_3 sample are more complicated than just the reaction to a bulk cobalt aluminate layer in the upper layer of the

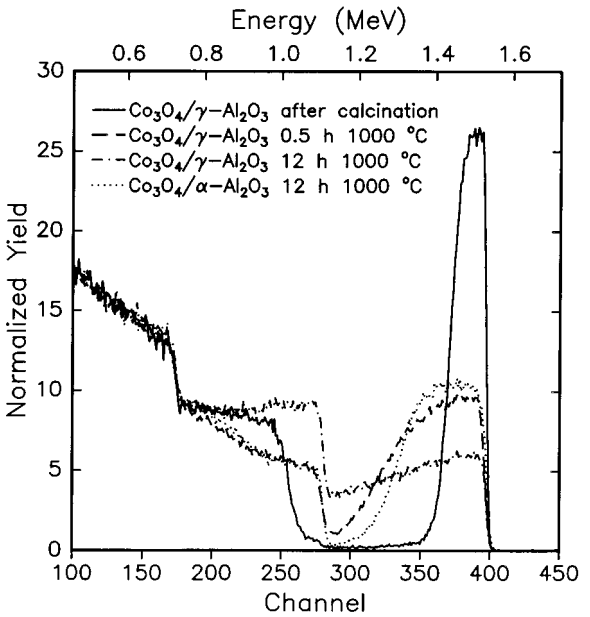

FIG. 3. RBS spectra of Co_3O_4/γ-Al_2O_3 annealed at 1000°C in N_2/20% O_2 for 0, 0.5, and 12 h and Co_3O_4/α-Al_2O_3 annealed at 1000°C for 12 h. The thickness of the deposited Co films amounted to about 45 nm. Beam: 2.01-MeV He^+.

sample. It is noteworthy that α-Al_2O_3 peaks were found in the X-ray diffraction pattern of this sample. Moreover, SEM images of Co_3O_4/γ-Al_2O_3 samples kept at 1000°C (not shown) demonstrated that the surface of these samples was considerably smoother than that of unannealed samples, which is likely to be related to the transition of γ-Al_2O_3 to α-Al_2O_3.

Influence of the oxygen partial pressure. Two Co_3O_4/α-Al_2O_3 samples kept at 1000°C for 3 h in high-purity N_2 and in 100% O_2, respectively, showed no significant difference in the rate of cobalt aluminate formation. This is not unexpected, since CoO is the stable cobalt oxide at 1000°C in both 1 atm O_2 and high-purity N_2 (13, 14). The fact that the O_2-annealed sample contained Co_3O_4 instead of CoO is explained by reoxidation of CoO during the cooling period.

When two Co_3O_4/γ-Al_2O_3 samples were annealed at 850°C for 10 h, the N_2-annealed sample exhibited significantly more interdiffusion of cobalt and aluminum ions than the O_2-annealed sample (not shown). This difference could be related to the oxygen potential-dependent thermodynamic stability of the cobalt oxides. CoO is the stable cobalt oxide at 850°C in high-purity N_2. According to Oku and Sato (13), Co_3O_4 is the stable oxide in 1 atm O_2 at temperatures below 950°C, but from the data of Barin and Knacke (14), a Co_3O_4–CoO transition temperature of 825°C was calculated.

Nickel Oxide on Alumina

Figure 4 shows the RBS spectra of NiO samples after annealing at 1000°C in N_2/20% O_2. The spectra are similar to those of the Co_3O_4/α-Al_2O_3 samples (Fig. 1b), but now much longer annealing periods are required to achieve the same extent of aluminate formation. Formation of bulk $NiAl_2O_4$ was proven by XRD, and after complete reaction the samples were pale blue, the characteristic color of $NiAl_2O_4$.

Similarly to the Co_3O_4/Al_2O_3 system, interdiffusion of Ni^{2+} and Al^{3+} was found to occur much faster in NiO/γ-Al_2O_3 than in NiO/α-Al_2O_3 samples (not shown). However, bulk nickel aluminate could not be detected in annealed NiO/γ-Al_2O_3 samples with XRD, and the samples were green instead of pale blue.

No influence of the oxygen partial pressure on NiO/Al_2O_3 samples was found. This is not surprising, since NiO is the only stable nickel oxide.

Copper Oxide on Alumina

The RBS spectra of CuO/α-Al_2O_3 samples annealed at 1000°C in 100% O_2 are presented in Fig. 5. Obviously, the CuO/α-Al_2O_3 samples exhibit a behavior different from that of Co_3O_4/α-Al_2O_3 or NiO/α-Al_2O_3 samples. No shoulder is visible at the low-energy side of the copper peak in the RBS spectra of the annealed CuO/α-Al_2O_3 samples, but there is a long diffusion tail extending to lower energies. When

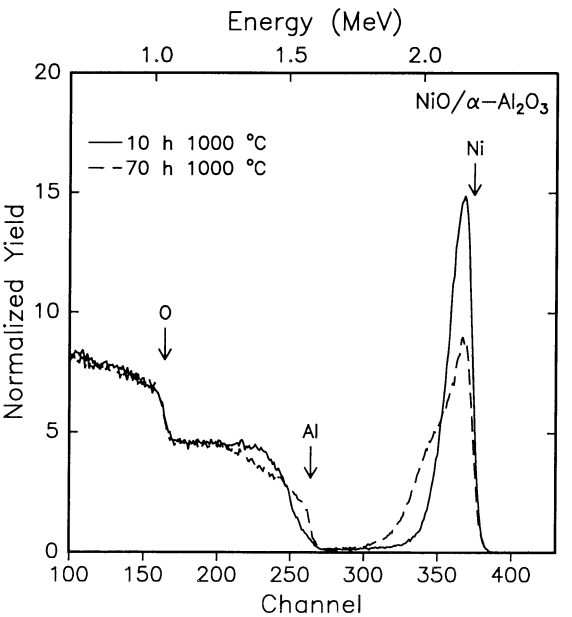

FIG. 4. RBS spectra if NiO/α-Al_2O_3 samples after annealing at 1000°C in N_2/20% O_2 for 10 and 70 h. The thickness of the deposited Ni films amounted to about 60 nm.

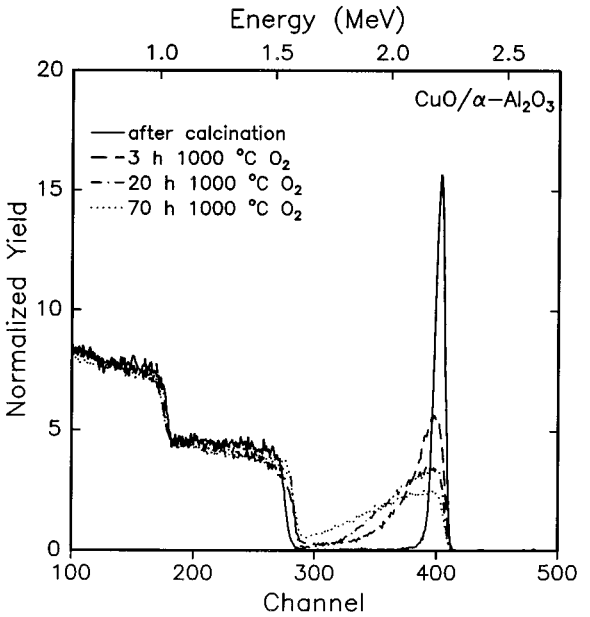

FIG. 5. RBS spectra of CuO/α-Al_2O_3 samples recorded after annealing at 1000°C in 100% O_2 for 0, 3, 20, and 70 h. The thickness of the deposited Cu films amounted to 35 nm.

Fig. 5 is compared to Figs. 1b and 4, it appears that copper ions penetrate much faster and deeper into the α-Al_2O_3 substrate than cobalt or nickel ions. Moreover, the Cu/Al ratio at the sample surface dropped far below the 1/2 ratio upon annealing at 1000°C and did not reach a stable value. After 70 h of annealing at 1000°C in O_2 (Fig. 5), the Cu/Al ratio at the surface was 1/7; yet XRD only revealed diffraction peaks of α-Al_2O_3 and $CuAl_2O_4$. The positions of the $CuAl_2O_4$ peaks were slightly shifted to lower lattice spacings, which may be attributed to the dissolution of some excess Al_2O_3 in the copper aluminate. Samples kept at 1000°C for a relatively short period (3 h) were brown, but after long annealing periods they were orange. The origin of the orange color is not known; $CuAl_2O_4$ is chocolate brown and CuO dark brown to black.

Figs. 6a and 6b show SEM images of a calcined CuO/α-Al_2O_3 sample and of a sample kept at 1000°C for 70 h, respectively. Clearly, the heat treatment at 1000°C resulted in destruction of the structure of the sample surface. The crystallites at the surface of the sample are much smaller than the original α-Al_2O_3 grains, which are still vaguely visible underneath the smaller particles. This change of the sample surface morphology, which involves mass transport over considerably large distances, could explain why no shoulder at the copper peak but rather a fast and deep penetration of copper atoms is observed in the RBS spectra of annealed CuO/α-Al_2O_3 samples. EDX analysis indicated that the lateral distribution of the copper atoms was still homogeneous on the scale of the micrographs.

SEM revealed that even with CuO/α-Al_2O_3 $(11\bar{2}0)$ samples, the surface of the α-Al_2O_3 $(11\bar{2}0)$ single crystal was severely disrupted after annealing at 1000°C in O_2. However, it appeared that considerably longer annealing periods were required in the latter case to obtain the same depth distribution of copper.

Similarly as with the Co_3O_4/α-Al_2O_3 system (at 850°C) it was found that the penetration of copper ions into α-Al_2O_3 occurs even faster in N_2 than in O_2 (at 1000°C). At this temperature CuO is the stable copper oxide in 1 atm O_2, whereas Cu_2O is the stable oxide in high-purity N_2 (14). In both cases the only observed reaction product was $CuAl_2O_4$; $CuAlO_2$ diffraction peaks were not detected.

Figure 7 shows the RBS spectra of some CuO/γ-Al_2O_3 samples annealed for 3 h at 700–900°C in 100% O_2. The oxidation of the copper layer prior to the annealing experiments had taken place at 500°C (12 h). Even at this temperature, some diffusion of copper into the support had occurred, as is evidenced by the tail at the low-energy side of the copper peak (solid curve). This diffusion tail was more pronounced after further annealing at 500°C (dashed curve). At 700°C the copper atoms rapidly penetrated into the γ-Al_2O_3 substrate. Just as with α-Al_2O_3 substrates, no shoulder is visible at the low-energy side of the copper peak. Instead, a sharp peak is present at the surface energy position of copper, and a long, virtually linear tail extends to energies lower than the surface energy position of aluminum, which means that copper has penetrated deeply (more than 1 μm) into the substrate. Upon annealing at 800°C, the sharp peak disappeared and the slope and intensity level of the tail decreased. This indicates that copper had diffused even further into the alumina. After annealing at 900°C, the copper had penetrated the substrate so deeply that the Cu/Al ratio at the surface (and the first micron) was only 1/47. No $CuAl_2O_4$ or any other copper compound could be detected with XRD in the annealed CuO/γ-Al_2O_3 samples; only the γ-Al_2O_3 diffraction peaks were visible. The samples did not have the chocolate-brown color of $CuAl_2O_4$; the samples annealed for 3 h at 800 and 900°C were green, and the sample kept at 700°C was dark brown with green spots. SEM images of these samples did not show any difference with unannealed samples.

Iron Oxide on Alumina

Little interdiffusion of Fe and Al ions was observed (Fig. 8) after annealing a Fe_2O_3/α-Al_2O_3 sample for 70 h at 1000°C in either 100% O_2 or 100% N_2. However, some Al has penetrated into the overlayer, as evidenced by the step in the Al edge, with the N_2-annealed sample showing a higher Al concentration than the O_2-annealed sample. XRD measurements revealed that, during the N_2 annealing, Fe_2O_3 was converted into Fe_3O_4, while only Fe_2O_3 could be observed in the diffractogram of the O_2-annealed sample.

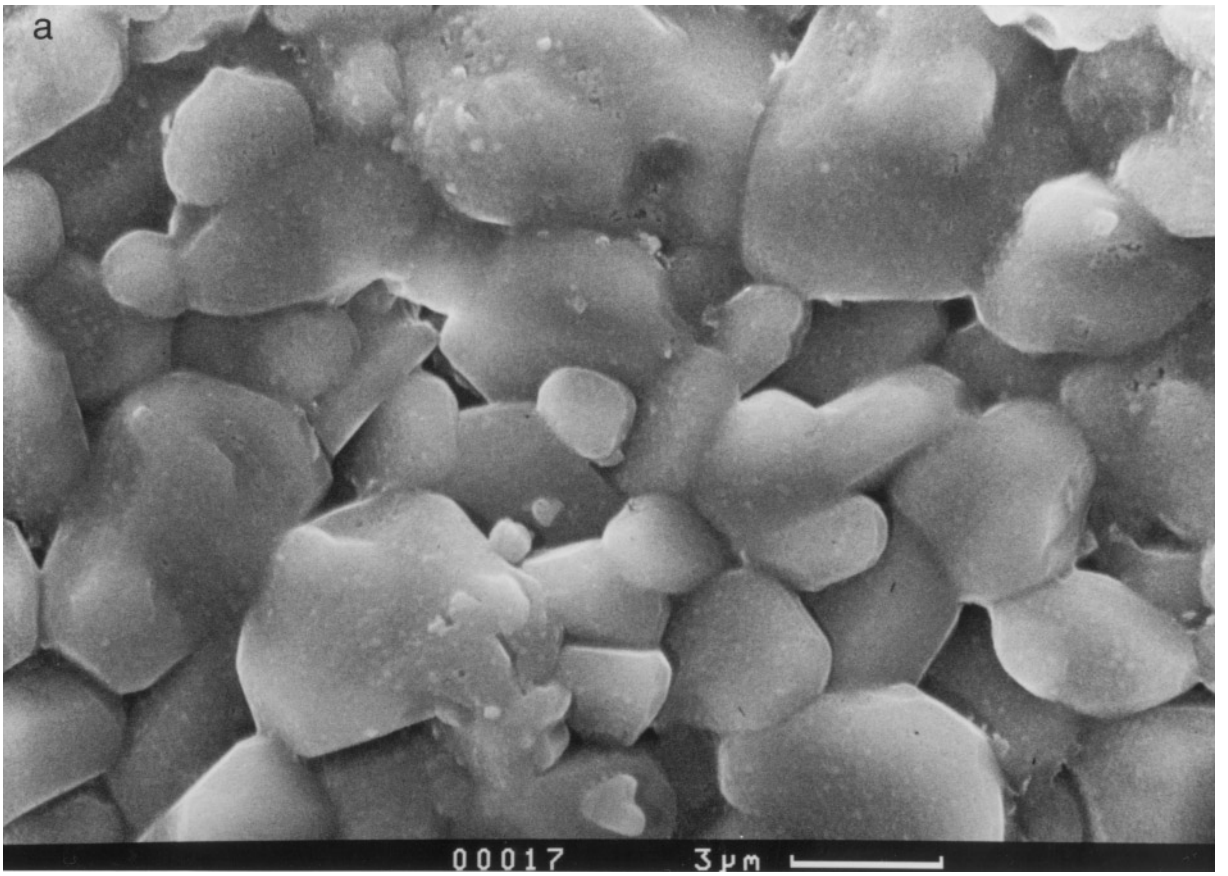
a
00017
3µm

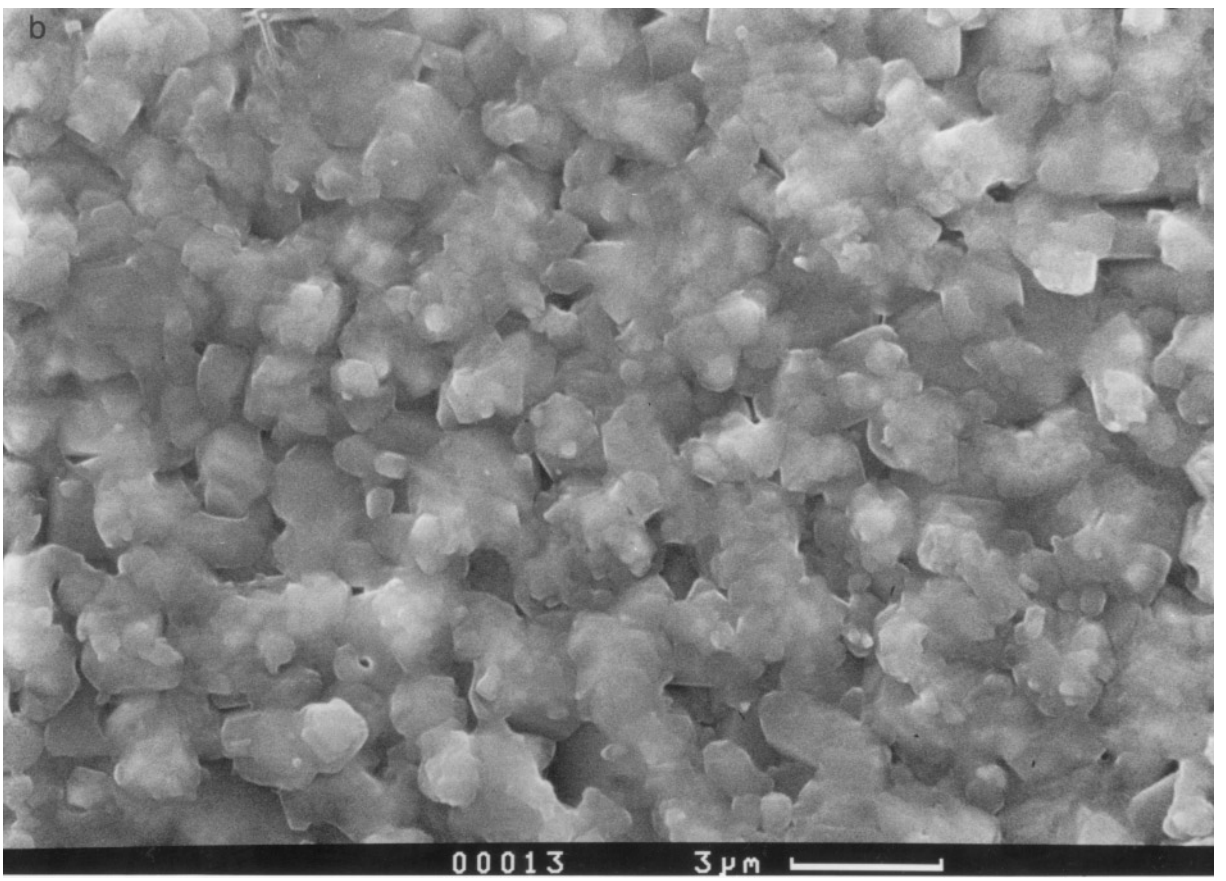
b
00013
3µm

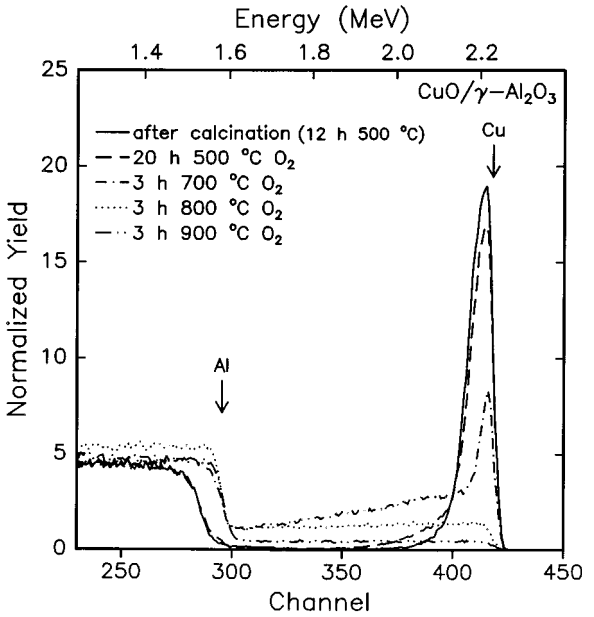

FIG. 7. RBS spectra of CuO/γ-Al_2O_3 samples kept after calcination (for 12 h at 500°C in N_2/20% O_2) and after annealing for 3 h in 100% O_2 at 700, 800, and 900°C. The thickness of the deposited Cu films amounted to about 50 nm.

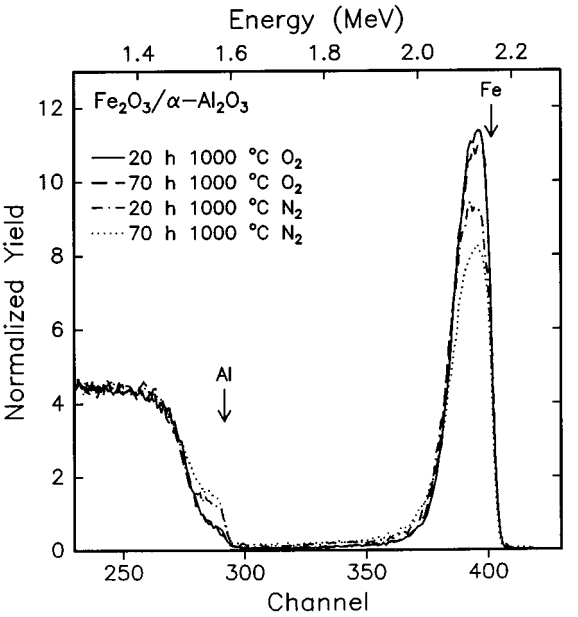

FIG. 8. RBS spectra of Fe_2O_3/α-Al_2O_3 samples kept at 1000°C for 20 or 70 h in 100% O_2 and 100% N_2. The thickness of the deposited Fe films amounted to about 45 nm.

These observations can be explained by thermodynamic considerations. At 1000°C Fe_2O_3 is the stable iron oxide in 1 atm O_2, and Fe_3O_4 in high-purity N_2. Fe–Al–O phase diagrams (15) show that some Al_2O_3 can be dissolved in Fe_2O_3 and vice versa, but any further interaction of Fe_2O_3 with Al_2O_3 is not likely to occur. This explains the shape of the solid curve in Fig. 8. Pure $FeAl_2O_4$ is stable only at very low oxygen partial pressures (lower than 10^{-10} atm), which are not realized at 1 atm in high-purity (99.999%) N_2 flows. There is a very wide solubility range of $FeAl_2O_4$ and Fe_3O_4, but the minimum value of x in $FeAl_2O_4 \cdot xFe_3O_4$ depends on the oxygen partial pressure. This is likely to determine the shape of the dotted curve in Fig. 8.

DISCUSSION AND CONCLUSIONS

General Considerations

The rate of a reaction between two solids is controlled either by the chemical reaction itself or by diffusion of (one of) the reactants. Especially at low temperatures, nucleation of the reaction product often acts as a kinetic barrier in the first stage of solid-state reactions. The results discussed in a previous paper (9) provide evidence that the solid-state reaction between NiO and α-$Al_2O_3(11\bar{2}0)$ single crystals is controlled by nucleation of the reaction product $NiAl_2O_4$ at temperatures up to 950°C.

When as a result of the solid-state reaction an intermediate layer of the reaction product is created between the reactants, the reaction can only continue by diffusion of (one of) the reactants through the reaction product if gas-phase transport is precluded. In the case of the reaction to transition metal aluminates, $MeAl_2O_4$, counterdiffusion of Al^{3+} and Me^{2+} through the spinel layer occurs (2, 5, 8). When the thickness of the intermediate $MeAl_2O_4$ layer is sufficiently large, the reaction rate is controlled by this diffusion process. In this case, the kinetics can be described by the parabolic growth rate law, which implies that the thickness of the spinel layer increases with the square root of the annealing time (2, 5, 8).

However, before this stage of the reaction is reached, when the intermediate layer of the reaction product is still relatively thin, the reaction kinetics shows a more complex behavior. This is also the case when ions of one reactant penetrate the other reactant (and vice versa) by diffusion along grain boundaries and the surfaces of internal pores, but no (three-dimensional) bulk reaction product is formed

FIG. 6. SEM images of CuO on polycrystalline α-Al_2O_3 (Gimex) (a) after calcination (at 700°C) and (b) after annealing at 1000°C in 100% O_2 for 70 h. The thickness of the deposited Cu films amounted to about 35 nm.

(yet). This pertains usually to the early reaction stages when grain boundaries are present and the nucleation of the reaction product is slow (i.e., at relatively low temperatures), since the mobility of species at the surface of a grain is considerably higher than in the bulk. In this situation, the interaction between the reactants is confined to the first (few) monolayer(s) of their grains, which may be described as a solid-state reaction to a (two-dimensional) surface compound. In studies on alumina-supported transition metal oxides, such "surface spinel species" have been reported frequently (16, 17). Such species exhibit structural, spectroscopic, and chemical similarities with bulk spinels but are not detectable with XRD.

In later stages of the reaction these surface compounds may grow out into a bulk reaction product. The reaction front will then advance toward the center of the grains both from the grain boundaries and from the original interface of the reactants (6). After some time the reaction will be controlled by diffusion through a bulk reaction product, and thus the overall reaction rate will obey the parabolic growth rate law. In this situation, the presence of grain boundaries does not change the kinetics of the reaction; it just makes the reaction faster (18).

Transition Metal Oxides on α-Alumina: Thermodynamic Limitations

The reaction rate of MeO_x(Me = Ni, Co, Cu, Fe) with alumina to $MeAl_2O_4$ was found to follow the sequence $FeAl_2O_4 < NiAl_2O_4 < CoAl_2O_4 < CuAl_2O_4$.

The low reactivity of iron oxides with alumina in either 1 atm O_2 or N_2 is explained by thermodynamic considerations. Fe_2O_3 (hematite) is the thermodynamically stable iron oxide at 1000°C in 1 atm O_2, which can dissolve some Al_2O_3 but does not react to $FeAl_2O_4$ (hercynite). In 1 atm high-purity N_2, Fe_3O_4 (magnetite) is the stable iron oxide. It reacts with Al_2O_3 to a mixed hercynite–magnetite compound ($FeAl_2O_4 \cdot xFe_3O_4$); the minimum value of x depends critically on the oxygen partial pressure (15).

We thus conclude that the relative stability of Fe^{3+} with respect to Fe^{2+} protects FeO_x/Al_2O_3 model systems from $FeAl_2O_4$ formation. The stability of metal oxidation states higher than $+2$ suppresses spinel formation in several other MeO_x/Al_2O_3 systems, for example in MnO_x/Al_2O_3 (19).

Transition Metal Oxides on α-alumina: Diffusion through an Aluminate Layer

The difference in the rate of the reactions to nickel, cobalt, and copper aluminate, however, must be explained on the basis of other factors. In these cases, the formation of a bulk aluminate was demonstrated by XRD, and indications were found that parabolic growth rate law applied at least in the cases of nickel oxide (6, 8) and cobalt oxide (Fig. 2) overlayers on α-Al_2O_3. We therefore assume that the rate of the reaction was controlled by diffusion of ions through a bulk spinel layer.

The diffusion mechanism of solid-state spinel formation is the counterdiffusion of cations through a nearly immobile and approximately close-packed anion array (2, 5, 18, 20–22). According to the literature (18, 20–22), the corresponding kinetics depends mainly on two factors: cation size and site-preference energy. With the elements considered in this study, the first of these factors probably does not have a large influence, because the sizes of the Ni^{2+}, Co^{2+}, and Cu^{2+} cations are comparable. The second factor, site-preference energy, refers to the energy changes involved in the diffusion of metal ions through a series of alternating tetrahedral and octahedral vacancies. In the anion sublattice of the spinel there are eight adjacent tetrahedral interstices for each octahedral site and four adjacent octahedral interstices for each tetrahedral site (2). Only 50% of the octahedral and 12.5% of the tetrahedral vacancies are occupied by cations. This allows a voidal diffusion path, as pointed out by Azaroff (23). A small (or zero) energy change between tetrahedral and octahedral coordination enhances the mobility of the cation involved. In contrast, a strong preference for either octahedral or tetrahedral sites leads to a lower diffusion rate. In agreement with these predictions, Fernandez Colinas and Otero Arean (22) reported that the rates of spinel formation followed the sequence $NiAl_2O_4 < ZnAl_2O_4 < MgAl_2O_4$ (at 1100°C in air). The low rate for the reaction to $NiAl_2O_4$ is attributed to the high octahedral site-preference energy of the Ni^{2+} ion (about 50 KJ/mol) (24). $MgAl_2O_4$ forms considerably faster than $ZnAl_2O_4$, because the radius of the Zn^{2+} ion is about 12% larger than that of Mg^{2+}, and, more significantly, Zn^{2+} has a strong tetrahedral site preference (about 32 kJ/mol), whereas Mg^{2+} shows a very little site preference in spinel oxides (24).

In contrast to these results, Stone and Tilley (20) did not observe a substantial difference in the rates of $MgAl_2O_4$ and $ZnAl_2O_4$ formation. The rate sequence they found was $NiAl_2O_4 < MgAl_2O_4 \approx ZnAl_2O_4 < CuAl_2O_4$. Recently, Fernandez Colinas and Otero Arean (22) explained this discrepancy by arguing that Stone and Tilley performed their experiments at such high temperatures (1200°C) that volatilization of ZnO brings about a reaction route involving gas-phase transport, which considerably increases the reaction rate.

The higher rate of the reaction to $CoAl_2O_4$ as compared to that to $NiAl_2O_4$, which was observed in our experiments, is in agreement with the predictions of the site-preference energy concept. The Co^{2+} ion has only a weak tetrahedral site preference (about 13 kJ/mol), while Ni^{2+} has a strong octahedral site preference (about 50 kJ/mol) (24). However, the reaction of Al_2O_3 with CuO was even faster than with cobalt oxide, although Cu^{2+} also has a strong octahedral site preference (about 38 kJ/mol).

The surprisingly fast reaction to $CuAl_2O_4$ has also been found by Stone and Tilley (20). These authors suggested that this could be related to tetragonal (Jahn–Teller) distortion. However, in our study it was shown by SEM (Fig. 6) that the reaction of CuO and α-Al_2O_3 was accompanied by a destruction of the structure of the upper layer (~ 1 μm) of the substrate, which will be discussed shortly. It is likely that this resulted in a huge increase of the contact area between copper oxide and alumina, which probably accounts for the relatively high rate of copper aluminate formation, rather than a high diffusion constant of Cu^{2+}. The overall reaction was thus for a large amount of CuO in the reaction-controlled regime.

Grain Boundaries

The site-preference energy concept does not account for several other observations in this study. These observations include the enormously higher reactivity of γ-Al_2O_3 with respect to α-Al_2O_3, the unexpected green color of annealed CuO/γ-Al_2O_3 samples, the relatively high reaction rates of MeO_x/Al_2O_3 samples (Me = Co, Cu) at low oxygen potentials, and the different behavior of α-Al_2O_3-supported CuO. We judge it reasonable to suggest that most of these findings are associated with the effects of grain boundaries and other defects.

The important role of grain boundaries in the transition metal oxide overlayer is demonstrated by the presence of some aluminum atoms at the surface of the sample after the initial stage of the solid-state reaction (see, for example, Fig. 1). Consistently, in a previous study (8) it was found that the rate of $NiAl_2O_4$ formation at 1020°C was in NiO/$Al_2O_3(11\bar{2}0)$ samples about twice as high as in NiO/polycrystalline α-Al_2O_3 samples, which was attributed to a lower grain boundary density in the NiO layer in the latter case.

CuO/α-Alumina

The influence of the grain boundaries in polycrystalline α-Al_2O_3 is manifest in the case of CuO/α-Al_2O_3 samples. Deep penetration of copper atoms was accompanied by severe reconstruction of the top layer of the sample (about 1 μm deep) during annealing at 1000°C, which resulted in the formation of new particles on the surface of the sample, which were not enriched or depleted with copper atoms with respect to the overall composition of the surface layer. This process took place both on α-$Al_2O_3(11\bar{2}0)$ single crystals and on polycrystalline α-Al_2O_3 substrates, but the rate of this reconstruction process was substantially higher on polycrystalline α-Al_2O_3. Although the fundamentals of this process are not well understood, it is obvious that the presence or absence of grain boundaries in the substrate plays an important role. This observation supports the assumption that the high rate $CuAl_2O_4$ formation (as compared to the reactions to $CoAl_2O_4$ and $NiAl_2O_4$) is related to the drastic roughening of the sample surface rather than a possibly high mobility of Cu^{2+} in bulk $CuAl_2O_4$.

The observed peculiar roughening of CuO/α-Al_2O_3 samples may be related to the Cu–Al–O phase diagrams (25). Two stable copper aluminates exist: $CuAl_2O_4$, which is unstable with respect to CuO and α-Al_2O_3 below 612°C, and $CuAlO_2$. $CuAlO_2$ is unstable with respect to $CuAl_2O_4$ in air at temperatures below 1000°C, and in the presence of excess Al_2O_3 below 1170°C. In 1 atm O_2 these transition temperatures are higher, and in 1 atm N_2, of course, lower. Cu_2O is unstable with respect to CuO in air below 1026°C (below 1116°C in 1 atm O_2), so CuO was the stable copper oxide under reaction conditions in the case of our O_2-annealed samples. However, Oku and Sato (13) reported that the transition of Co_3O_4 to CoO occurred in the near-surface region already at temperatures 200°C lower than the temperatures predicted by bulk thermodynamic values. Similarly, the presence of some Cu^+ on the surface of the CuO grains may be expected at 1000°C in 1 atm O_2. This may give rise to the formation of a metastable $CuAlO_2$ phase, which is subsequently converted into $CuAl_2O_4$. The formation and dissociation of a metastable compound might explain the appearance of a very rough sample surface.

This explanation is supported by the observation that the same copper depth distribution is obtained within a shorter annealing period when the thermal treatment at 1000°C was carried out in N_2. Under these conditions, Cu_2O is the stable copper oxide, so more Cu^+ is available, and $CuAlO_2$ is now stable when there is locally no excess of alumina present (i.e., at the copper oxide/copper aluminate interface).

Rough interfaces in Cu–Al–O systems have also been reported by other authors. Susnitzky and Carter (26) embedded single-crystalline and polycrystalline α-Al_2O_3 substrates in copper oxide powder and annealed them at 1100–1300°C in air for long periods of time (72–1500 h). They observed a rather complex behavior of the Cu–Al–O system: Both $CuAl_2O_4$ and $CuAlO_2$ were found to coexist with Cu_2O and α-Al_2O_3. The interfaces between these phases were wavy and facetted, and $CuAl_2O_4$ particles were present within the $CuAlO_2$ layer. Such complex behavior was also reported by Mellul and Chevalier (27) for Cu/Cu_2O/α-Al_2O_3 samples annealed at 950°C in Ar. In both papers the results were discussed with reference to Cu–Al–O phase diagrams.

Transition Metal Oxides on γ-Alumina

Because of its much higher grain boundary density, its "defect spinel structure", which closely resembles the structure of the reaction product, and its thermodynamic metastability, γ-Al_2O_3 is expected to react faster to aluminates

than α-Al_2O_3. These expectations have proven to be true; penetration of *Me* atoms (*Me* = Ni, Co, Cu) into γ-Al_2O_3 substrates occurred enormously more rapidly than into α-Al_2O_3 substrates.

Several results of this study provide evidence for the assumption that, especially at relatively low annealing temperatures, diffusion of *Me* ions largely takes place along the grain boundaries and the surfaces of the internal pores of the γ-Al_2O_3. At higher annealing temperatures (about 900–1000°C) diffusion into the bulk of the alumina grains also occurs, resulting in aluminate formation, as observed using XRD.

The results are as follows:

(i) The *Me* peaks in the RBS spectra of annealed MeO_x/γ-Al_2O_3 samples exhibit a long tail toward lower energies, indicating that a significant fraction of *Me* ions penetrated rather deeply into the substrate. The CuO/γ-Al_2O_3 system is the most extreme example of this behavior (Fig. 7); in this case, diffusion of copper ions was already notable at 500°C.

(ii) At 800°C the Co_3O_4/γ-Al_2O_3 system did not obey the parabolic growth rate law; while considerable cobalt diffusion was observed in the first annealing period of 20 h, little happened in the next 20 h. Since the γ-Al_2O_3 grain boundaries serve as a deep potential sink for the cobalt ions, it is expected that these cobalt ions initially rapidly diffuse into the grain boundaries. After some time, however, when the boundaries of the alumina grains in the near-surface region of the sample are decorated with cobalt ions and the temperature is too low for noticeable diffusion into the bulk of the grains, the rate of the diffusion process diminishes, because of the decreasing driving force.

(iii) While sharp peaks originating from metal aluminates were visible in the XRD patterns of annealed MeO_x/α-Al_2O_3 samples, usually no spinel diffraction peaks could be discerned with annealed MeO_x/γ-Al_2O_3 samples. This means that no large $MeAl_2O_4$ particles were formed on the γ-Al_2O_3 slices, in contrast to the α-Al_2O_3 substrates. Apparently, the spinel particles are too small to give rise to diffraction peaks that are discernible from the broad γ-Al_2O_3 peaks, or the solid-state reaction is confined to the first (few) monolayer(s) of each γ-Al_2O_3 grain in the surface region of the substrates. Therefore we suggest that the transition metal ions enter the cation vacancies in the first (few) monolayer(s) of the γ-Al_2O_3 grains but that the diffusion process is limited to these surface layers. Diffusion into the bulk of the grains is not significant, because the annealing temperature is too low or, especially in the case of CuO/γ-Al_2O_3 samples, because the formation of bulk aluminate cannot compete successfully with the extremely rapid diffusion along the grain boundaries.

(iv) From the RBS spectra of Co_3O_4/γ-Al_2O_3 and NiO/γ-Al_2O_3 samples kept at 1000°C (e.g., Fig. 3), it was derived that the Co/Al and Ni/Al ratios in the near-surface region of the samples dropped substantially below the value corresponding to the solubility limit of Al_2O_3 in the spinel compounds. This can be explained by rapid grain boundary diffusion in combination with a much slower bulk diffusion process. Some unreacted γ-Al_2O_3 remains in the core of the grains.

(v) After annealing a CuO/γ-Al_2O_3 sample at 900°C for 3 h, the copper atoms had penetrated the substrate so deeply that the Cu/Al ratio was only 1/47 at the surface of the sample, and no copper concentration gradient was visible in at least the first micron (Fig. 7). This can only be understood if the copper atoms are confined to the outermost layers of the γ-Al_2O_3 grains.

(vi) The green color of the annealed CuO/γ-Al_2O_3 samples can probably be attributed to the presence of copper ions in an octahedral coordination state, $Cu^{2+}O_6$ (28–30). Because this is not a bulk compound but a surface species, the copper atoms must be located on the surface of the internal pores and in the boundaries between the γ-Al_2O_3 grains.

From these findings it is clear that the high grain boundary density of γ-Al_2O_3 is a major reason for its high reactivity toward aluminate formation, as compared to α-Al_2O_3. The "defect spinel structure" of γ-Al_2O_3 may also have a beneficial effect on the solid-state reaction between transition metal oxides and γ-Al_2O_3; it will facilitate cations to enter the alumina lattice. Furthermore, the thermodynamic metastability of γ-Al_2O_3 should not be neglected. The specific surface area of the γ-Al_2O_3 substrate decreased substantially during annealing, and at 900–1000°C transition of γ-Al_2O_3 via θ-Al_2O_3 to α-Al_2O_3 occurred. Because of these solid-state transformations, an enhanced reactivity of the alumina is also expected (Hedvall effect).

ACKNOWLEDGMENTS

The authors thank the crew of the accelerator department of Utrecht University for running the accelerator. This work has been supported by the Stichting Scheikundig Onderzoek Nederland (SON).

REFERENCES

1. F. S. Pettit, E. H. Randklev, and E. J. Felten, *J. Am. Ceram. Soc.* **49,** 199 (1966).
2. J. S. Armijo, *Oxid. Met.* **1,** 171 (1969).
3. W. J. Minford and V. S. Stubican, *J. Am. Ceram. Soc.* **57,** 363 (1974).
4. K. Hirota and W. Komatsu, *J. Am. Ceram. Soc.* **60,** 105 (1977).
5. H. Schmalzried,"Solid State Reactions," 2nd ed. Verlag Chemie, Weinheim, 1981.
6. G. de Roos, J. H. W. de Wit, J. M. Fluit, J. W. Geus, and R. P. Velthuizen, *Surf. Interface Anal.* **5,** 119 (1983).
7. P. H. Bolt, S. F. Lobner, T. P. van den Bout, J. W. Geus, and F. H. P. M. Habraken, *Appl. Surf. Sci.* **70/71,** 196 (1993).
8. P. H. Bolt, S. F. Lobner, J. W. Geus, and F. H. P. M. Habraken, *Appl. Surf. Sci.* **89,** 339 (1995).

9. P. H. Bolt, E. ten Grotenhuis, J. W. Geus, and F. H. P. M. Habraken, *Surf. Sci.* **329,** 227 (1995).
10. M. A. Apecetche, M. Houalla, and B. Delmon, *Surf. Interface Anal.* **3,** 90 (1981).
11. P. Arnoldy and J. A. Moulijn, *J. Catal.* **93,** 38 (1985).
12. H. Schmalzried, *Z. Phys. Chem.* (*N.F.*) **28,** 203 (1961).
13. M. Oku and Y. Sato, *Appl. Surf. Sci.* **55,** 37 (1992).
14. (a) I. Barin and O. Knacke, "Thermochemical Properties of Inorganic Substances." Springer-Verlag, Berlin, 1973; (b) I. Barin, O. Knacke, and O. Kubaschewski, "Thermochemical Properties of Inorganic Substances–Supplement." Springer-Verlag, Berlin, 1977.
15. C. E. Meyers, T. O. Mason, W. T. Petusky, J. W. Halloran, and H. K. Bowen, *J. Am. Ceram. Soc.* **63,** 659 (1980).
16. P. A. Chernavskii and V. V. Lunin, *Kinet. Catal.* **34,** 470 (1993).
17. M. Lo Jacono, M. Schiavello, and A. Cimino, *J. Phys. Chem.* **75,** 1044 (1971).
18. F. C. Tompkins, "Reactivity of Solids, Proceedings of the 5th International Symposium, Munich, 1964" (G.-M. Schwab, Ed.), p. 3. Elsevier, Amsterdam, 1965.
19. D. van de Kleut, Utrecht University, 1994. Ph.D. Thesis.
20. F. S. Stone and R. J. D. Tilley, "Reactivity of Solids, Proceedings of the 5th International Symposium, Munich, 1964" (G.-M. Schwab, Ed.), p. 583. Elsevier, Amsterdam, 1965.
21. F. S. Stone and R. J. D. Tilley, "Reactivity of Solids, Proceedings of the 7th International Symposium, Bristol, 1972" (J. S. Anderson, M. W. Roberts, and F. S. Stone, Eds.), p. 262. Chapman and Hall, London, 1972.
22. J. M. Fernandez Colinas and C. Otero Arean, *J. Solid State Chem.* **109,** 43 (1994).
23. L. V. Azaroff, *J. Appl. Phys.* **32,** 1658 (1961).
24. A. Navrotsky and O. J. Kleppa, *J. Inorg. Nucl. Chem.* **29,** 2701 (1967).
25. K. T. Jacob and C. B. Alcock, *J. Am. Ceram. Soc.* **58,** 192 (1975).
26. D. W. Susnitzky and C. B. Carter, *J. Mater. Res.* **6,** 1958 (1991).
27. S. Mellul and J.-P. Chevalier, *Philos. Mag. A* **64,** 561 (1991).
28. M. C. Marion, E. Garbowski, and M. Primet, *J. Chem Soc., Faraday Trans.* **86,** 3027 (1990).
29. J. C. Summers and R. L. Klimisch, "Proceedings of the 5th International Congress on Catalysis, Miami Beach, 1972" (J. W. Hightower, Ed.), p. 293. North-Holland Publishing Co., Amsterdam, 1972.
30. E. Garbowski and M. Primet, *J. Chem. Soc., Chem. Commun.* 11 (1991).